EXTENSIONS OF THE SPALART–ALLMARAS TURBULENCE MODEL TO ACCOUNT FOR WALL ROUGHNESS

B. Aupoix [a] and P.R. Spalart [b]

[a]ONERA/DMAE Centre d'Études et de Recherches de Toulouse
B.P. 4025, 2, Avenue Édouard Belin 31055 Toulouse CEDEX 4, France
[b]Boeing Commercial Airplanes
P.O. Box 3707 Seattle, Washington 98124, USA

ABSTRACT

Extensions of the Spalart–Allmaras turbulence model to account for wall roughness were developed independently by Boeing and ONERA. They are rather simple, yield similar predictions, and are in fair agreement with experiments. Tests confirm the weakness of the "equivalent sand grain" approach, i.e. the uncertain accuracy of correlations to determine the sand-grain size. Some test cases reveal an incompatibility between the predicted effect of roughness on heat transfer and on skin friction. i.e., if the sand-grain size is adjusted for skin friction, the heat transfer will be too high.

KEYWORDS

Boundary Layer, Equivalent Sand Grain, Heat Transfer, Pressure Gradient, Skin Friction, Turbulence Modelling, Wall Roughness.

1 EXTENSION OF THE SPALART–ALLMARAS MODEL

1.1 Basic Spalart–Allmaras (S-A) model

The S-A turbulence model solves only one transport equation for the quantity $\tilde{\nu}$, which is equivalent to the eddy viscosity ν_t far from walls. The transport equation has been constructed empirically to reproduce flows of increasing complexity. The transport equation reads, neglecting transition terms, (Spalart and Allmaras, 1994):

$$\frac{D\tilde{\nu}}{Dt} = c_{b1}\tilde{S}\tilde{\nu} - c_{w1} f_w \left(\frac{\tilde{\nu}}{d}\right)^2 + \frac{1}{\sigma}\left[\text{div}\left(\tilde{\nu}\,\underline{\text{grad}}\,\tilde{\nu}\right) + c_{b2}\,\underline{\text{grad}}\,\tilde{\nu}\cdot\,\underline{\text{grad}}\,\tilde{\nu}\right] \quad (1)$$

where d is the distance to the nearest wall. The model has been tuned so that, close to solid surfaces but outside the viscous region, it fits the logarithmic region, i.e.

$$\tilde{\nu} = u_\tau \kappa d \qquad \tilde{S} = \frac{u_\tau}{\kappa d} \tag{2}$$

where u_τ is the friction velocity based upon the wall friction τ_w ($u_\tau = \sqrt{\tau_w/\rho}$) and κ the von Kármán constant. The turbulent viscosity ν_t is linked to the transported variable $\tilde{\nu}$ by

$$\nu_t = f_{v1}\tilde{\nu}, \qquad f_{v1} = \frac{\chi^3}{\chi^3 + c_{v1}^3}, \qquad \chi = \frac{\tilde{\nu}}{\nu} \tag{3}$$

and $\tilde{S}$ is linked to the vorticity S (which reduces to $|\frac{\partial u}{\partial y}|$ in thin shear flows), by

$$\tilde{S} = S + \frac{\tilde{\nu}}{\kappa d^2} f_{v2}, \qquad f_{v2} = 1 - \frac{\chi}{1 + \chi f_{v1}}. \tag{4}$$

Finally, f_w is a function of the ratio $r \equiv \tilde{\nu}/(\tilde{S}\kappa^2 d^2)$, and both equal unity in the log layer.

1.2 Modelling roughness effects

It is assumed that the roughness height is small compared with the boundary layer thickness so that, above the roughnesses, the flow is averaged over roughness elements the exact location of which is not accounted for. Two "macroscopic" strategies can then be used to account for wall roughness in Navier–Stokes computations, without solving the flow equations around each roughness element. In both strategies, the boundary of the calculation domain is smooth and the velocity boundary condition is zero.

- The "discrete element approach" accounts for the roughness by extra terms in the flow equations which represent the flow blockage due to the roughnesses and the drag and heat flux on roughness elements (see, e.g. Coleman et al. (1983) or Aupoix (1994) for the derivation of the equations). However, this approach requires drastic changes in the flow equations and has not been used in practical applications.
- The "equivalent sand grain approach" links the real roughness to an idealized roughness, with reference to Nikuradse's experiments (1933), the height of the equivalent sand grain being deduced from the real roughness shape with the help of empirical correlations, usually the correlation proposed by Dirling (1973) and Grabow and White (1975). The roughness effect is mimicked by increasing the turbulent eddy viscosity in the wall region to obtain higher skin friction and wall heat flux levels. Here again, two kinds of model can be considered:
  - Models in which the eddy viscosity is null at the boundary. They can be interpreted as models in which the virtual "wall" corresponds to the bottom of the roughnesses. The roughness correction then mainly acts through a reduction of the turbulence damping in the wall region.
  - Models in which the eddy viscosity is finite at the boundary. They can be interpreted as models in which the virtual "wall" is located among the roughnesses. Unpublished studies at ONERA have shown that this approach better accounts for small roughnesses.

The increase in skin friction due to wall roughness can be directly related to changes in the velocity profiles, as will be shown in figure 9 where the profile is plotted in wall variables i.e. the reduced velocity $u^+ = u/u_\tau$ versus the reduced wall distance $y^+ = yu_\tau/\nu$. For high enough Reynolds numbers, the logarithmic region and the wake are simply shifted compared to the smooth wall case. Accordingly, the roughness modifications of the models vanish in those regions. It must be

remembered that the edge value is

$$u_e^+ = \frac{u_e}{u_\tau} = \sqrt{\frac{2}{C_f}} \tag{5}$$

so that, to first order, as the wake shape is unaffected by roughness, the increase in the skin friction coefficient C_f is directly related to the shift Δu^+ of the profile.

Nikuradse (1933) provided relations between this shift Δu^+ and the reduced roughness height $h_s^+ = h_s u_\tau/\nu$ for the specific sand-grain roughnesses of various heights h_s he investigated. Note that for most types of "real-life" roughness, the sand-grain size h_s that has the same effect is several times larger than the depth of the grooves or other irregularities.

Therefore, good predictions can be achieved only if the shift Δu^+ of the velocity profile is reproduced for any reduced sand-grain roughness height h_s^+ *and* the equivalent sand grain roughness h_s is correctly estimated from the true shape of the considered rough surface.

1.3 Boeing's extension

This extension (Spalart, 2000) was designed to preserve the model behaviour in the wall region (equation 2) but a non-zero value of $\tilde{\nu}$ is now expected at the wall to mimic roughness effects. For that, the wall condition $\tilde{\nu} = 0$ is replaced by

$$\frac{\partial \tilde{\nu}}{\partial n} = \frac{\tilde{\nu}}{d} \tag{6}$$

where n is along the wall normal and the distance d has to be increased. The simplest way is to impose a shift $d = d_{min} + d_0$ where d_{min} is the distance to the wall and $d_0(h_s)$ a shift that will be adjusted.

For very rough surfaces, in the fully rough regime ($h_s^+ > 70$), Nikuradse has shown that the velocity profiles, in the logarithmic region, obey

$$u^+ = \frac{1}{\kappa} \ln \frac{y}{h_s} + 8.5 \tag{7}$$

As the roughness effect is strong, the eddy viscosity should be large compared to the gas viscosity even at the wall. Therefore, the momentum equation reduces to

$$u_\tau^2 = \nu_t \frac{\partial u}{\partial y} = u_\tau \ \kappa \ d \ \frac{\partial u}{\partial y}, \tag{8}$$

the solution of which reads

$$u^+ = \frac{1}{\kappa} \left[\ln \left(y^+ + d_0^+ \right) - \ln \left(d_0^+ \right) \right]. \tag{9}$$

Identification of these two velocity profile expressions yields

$$d_0 = \exp(-8.5\kappa) h_s \approx 0.03 h_s. \tag{10}$$

To achieve good predictions for smaller roughnesses, the f_{v1} function in equation (3) is altered by modifying χ as

$$\chi = \frac{\tilde{\nu}}{\nu} + c_{R1} \frac{h_s}{d}, \qquad c_{R1} = 0.5 \tag{11}$$

This definition and value of c_{R1} correspond to a dependence of Δu^+ on h_s^+ which is close to that given by Schlichting (1979) after Nikuradse.

The balance of the transport equation imposes that all terms have the same behaviour with respect to d as for smooth surfaces, so that the definition of $\tilde{S}$ is unchanged

$$\tilde{S} = S + \frac{\tilde{\nu}}{\kappa d^2} f_{v2}, \qquad f_{v2} = 1 - \frac{\frac{\tilde{\nu}}{\nu}}{1 + \frac{\tilde{\nu}}{\nu} f_{v1}} \tag{12}$$

There is a misprint in the expression of f_{v2} in Spalart (2000).

1.4 ONERA's extension

As previous unpublished ONERA studies have favored models using a finite value of the wall turbulent viscosity, especially for intermediate roughness heights, it was decided to impose such a value for $\tilde{\nu}$ to simulate wall roughness effects.

The required wall value was determined by solving the one-dimensional problem in the wall region. Neglecting advection, equation (1) reads, in wall variables, i.e. making terms dimensionless with the viscosity ν and the friction velocity u_τ

$$0 = c_{b1} \tilde{S}^+ \tilde{\nu}^+ - c_{w1} f_w \left(\frac{\tilde{\nu}^+}{d^+} \right)^2 + \frac{1}{\sigma} \left[\frac{\partial}{\partial y^+} \left(\tilde{\nu}^+ \frac{\partial \tilde{\nu}^+}{\partial y^+} \right) + c_{b2} \left(\frac{\partial \tilde{\nu}^+}{\partial y^+} \right)^2 \right] \tag{13}$$

while the momentum equation reduces to

$$\frac{\partial u^+}{\partial y^+} - < u'v' >^+ = (1 + \nu_t^+) \frac{\partial u^+}{\partial y^+} = 1 \tag{14}$$

At the wall, the value of $\tilde{\nu}^+$ is imposed. The other boundary condition is imposed far in the logarithmic region where equation (14) reduces to $\tilde{\nu}^+ = \nu_t^+ = \kappa y^+ - 1$. Equation (13) is solved using a pseudo-unsteady approach. The velocity gradient which appears through $\tilde{S}$ is deduced from equation (14). Once a solution is obtained for $\tilde{\nu}$ and $\tilde{S}$, the velocity profile can be deduced by simple integration, and the shift Δu^+ is determined.

It turned out that even imposing very large wall values for $\tilde{\nu}^+$ yielded small values of the velocity shift as the sink term $-c_{w1} f_w \left(\frac{\tilde{\nu}}{d} \right)^2$ in the transport equation became large and suppressed the effect of the imposed wall condition. A shift in the wall distance d has to be introduced. To be consistent with the behaviour over smooth walls, the distance d is expressed as:

$$d^+ = d^+_{min} + \frac{\tilde{\nu}^+_w}{\kappa} \tag{15}$$

where $\tilde{\nu}_w$ is the imposed wall value for $\tilde{\nu}$. For a given wall value $\tilde{\nu}^+_w$, the solution of the one-dimensional problem gives a shift Δu^+ which our goal is to relate, through Nikuradse's results, to a sand grain roughness h_s^+. What is really needed is the inverse, i.e. the wall viscosity value to impose for a given roughness. The results have been processed to give the following relations:

$$\begin{aligned}
1035.95 \le h_s^+ \qquad & \tilde{\nu}^+_w = 1.1066\,10^{-6}\, {h_s^+}^2 + 1.1949\,10^{-2}\, h_s^+ + 0.5630 = P \\
150.4 \le h_s^+ \le 1035.95 \qquad & \tilde{\nu}^+_w = P - 6.4762\,10^{-12}\, {h_s^+}^4 + 1.653\,10^{-8}\, {h_s^+}^3 - 1.279\,10^{-5}\, {h_s^+}^2 \\
& \qquad +9.66\,10^{-4}\, h_s^+ + 1.8067 \\
4.24 \le h_s^+ \le 150.4 \qquad & \tilde{\nu}^+_w = P + 1.72 - 2.8 \exp\left(-\frac{h_s^+}{23.3} \right) \\
h_s^+ \le 4.24 \qquad & \tilde{\nu}^+_w = 0
\end{aligned} \tag{16}$$

1.5 Comparison of the two extensions

Boeing's model only refers to the sand-grain roughness height, whereas ONERA's model also needs the friction velocity. This leads to different behaviours close to two-dimensional separation where the friction velocity tends towards zero. Boeing's model then predicts stronger effects of the wall roughness. It must be pointed out that ONERA's model leads to no numerical problem at separation: u_τ is null, and so is h_s^+ and hence $\tilde{\nu}_w$ and d_0.

Both extensions change the wall boundary condition, either imposing the wall value or providing a mixed condition. In both cases, the wall distance d is modified so that the model is non-local: the information about the shift d_0 has to be known, i.e. each field point has to be related to a point on the surface. Boeing's change of d is simpler in that it only depends upon the roughness height and remains the same during computational iterations. Finally, Boeing's model requires changing the expression of χ in the damping function f_{v1}.

2 VALIDATION

Both extensions have been implemented in ONERA's two-dimensional boundary layer code CLIC2 and compared to other roughness models (mixing length, $k-\varepsilon$ and $k-\omega$ type models) for various experiments. The results of other models, which are either irrelevant or very close to the present ones, are not given here for the sake of clarity of the figures. Only a selection of pertinent test-cases is reported. In all figures, the solid line corresponds to the prediction of the S-A model over a smooth wall, to highlight roughness effects.

2.1 Blanchard's experiments

Blanchard (1977) conducted experiments over various surfaces, including sand grain paper of various heights and wire meshes. We present predictions for a sand grain paper the average height of which is 0.425mm. Blanchard estimated that the equivalent sand grain roughness height was twice the height of his roughness. This is not fully consistent with the equivalent sand grain roughness which can be deduced from Dirling's correlation and the simplified surface representation Blanchard proposed using cones, but he pointed to the large scatter in the correlation.

The first case corresponds to a zero pressure gradient flow, with an external velocity of 45ms^{-1}. This gives a reduced equivalent sand grain roughness height h_s^+ about 150, i.e. a fully rough regime. After a transient due to the initialization procedure, both models predict a skin friction evolution in fair agreement with experiments as shown in figure 1. Boeing's extension gives slightly higher predictions. For a rougher surface, velocity profiles predicted by both extensions are indistinguishable and in fair agreement with experiments. Figure 2 shows predictions for a positive pressure gradient flow. As the pressure gradient is moderate, the reduced equivalent sand grain roughness height h_s^+ remains about 150. The agreement with experiment remains good and the discrepancy between the models is reduced.

2.2 Acharya et al. experiments

Acharya et al. (1986) conducted experiments on surfaces specifically machined to reproduce aged turbine blade surfaces. Two surfaces, named SRS1 and SRS2 for "Simulated Rough Surface" have been considered, for a constant external velocity of 19ms^{-1}. Equivalent sand grain roughness

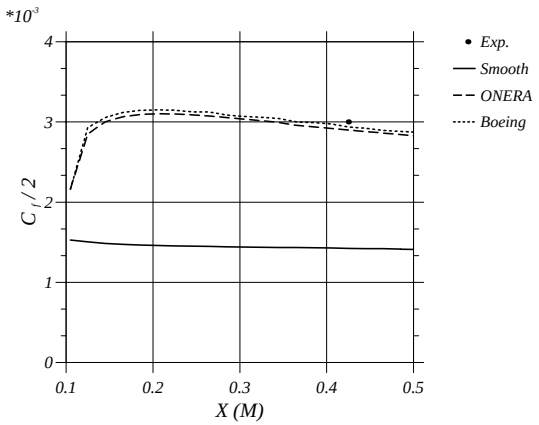

Figure 1: Skin friction predictions – Blanchard 0.425mm case – Zero pressure gradient flow

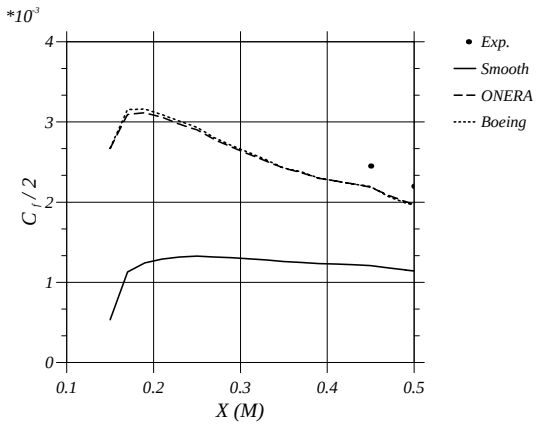

Figure 2: Skin friction predictions — Blanchard 0.425mm case – Positive pressure gradient flow

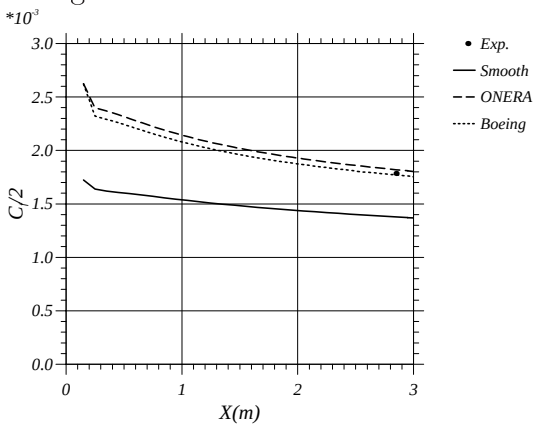

Figure 3: Skin friction predictions – Acharya et al. SRS1 Surface – U = 19ms^{-1} – Zero pressure gradient

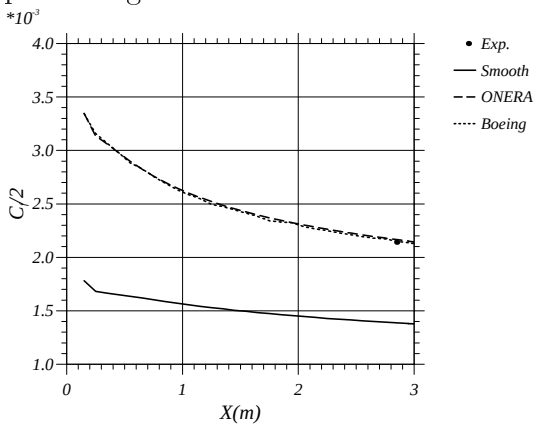

Figure 4: Skin friction predictions – Acharya et al. SRS2 Surface – U = 19ms^{-1} – Zero pressure gradient

heights have been evaluated from Dirling's correlation and surface statistics given in Tarada's thesis (1987).

Surface SRS1 gives a reduced equivalent sand grain roughness height h_s^+ about 25, i.e. a transitionally rough regime. Figure 3 shows that both models predict the skin friction fairly well, ONERA's model giving higher values and therefore better agreement. Surface SRS2 gives a reduced equivalent sand grain roughness height h_s^+ about 70, i.e. the lower limit of the fully rough regime. Figure 4 shows that both models are in excellent agreement with experiments.

2.3 MSU experiments

Many experiments over rough surfaces have been performed at the Mississippi State University (MSU). Hosni et al. (1991, 1993) investigated boundary layers over spheres, hemispheres and cones arranged in staggered rows in a low-speed wind tunnel designed to perform heat transfer measurements. Skin friction was deduced from the Reynolds stress $< -u'v' >$ above the roughnesses, corrected via a momentum balance around the roughnesses. The data were in fair agreement with the skin friction estimate from the von Kármán equation. Heat fluxes were deduced from an energy balance for each heated wall plate, accounting for losses by conduction and radiation. Only results for hemispheres, 1.27mm in diameter, will be presented here. The case of a spacing-over-height ratio of ten, i.e. for a weakly rough surface, is not presented here. All tests cases are for zero pressure

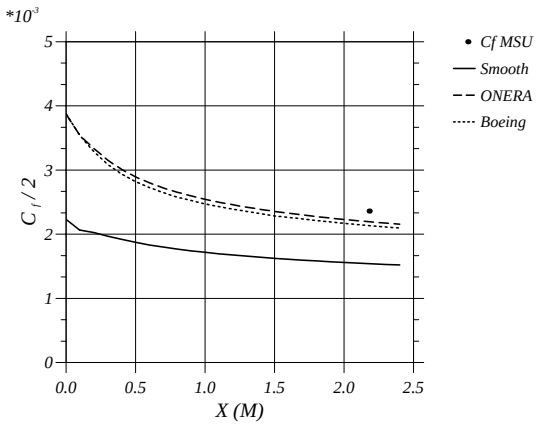

Figure 5: Skin friction predictions – MSU experiment – Hemispheres with spacing/height ratio of two – U = 12ms^{-1}

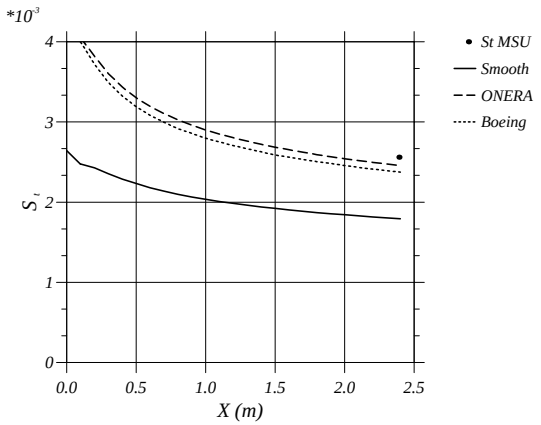

Figure 6: Stanton number predictions – MSU experiment – Hemispheres with spacing/height ratio of two – U = 12ms^{-1}

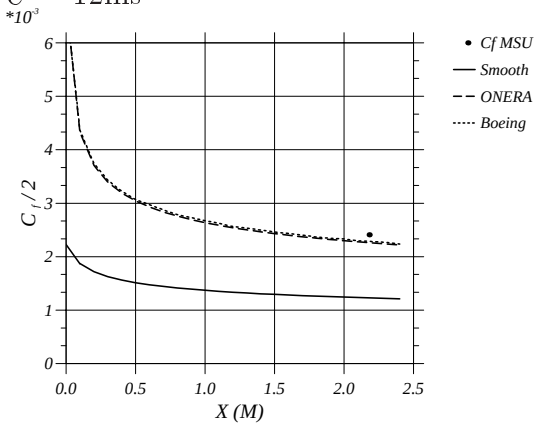

Figure 7: Skin friction predictions – MSU experiment – Hemispheres with spacing/height ratio of two – U = 58ms^{-1}

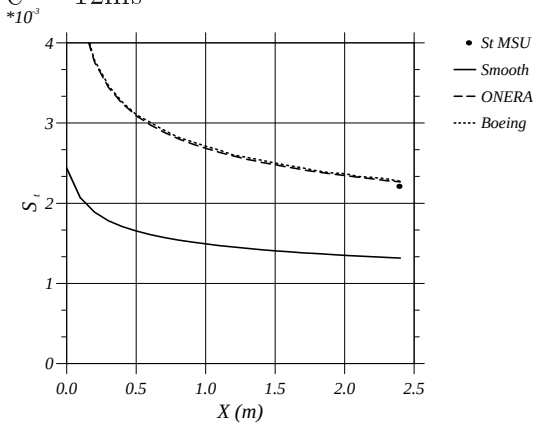

Figure 8: Stanton number predictions – MSU experiment – Hemispheres with spacing/height ratio of two – U = 58ms^{-1}

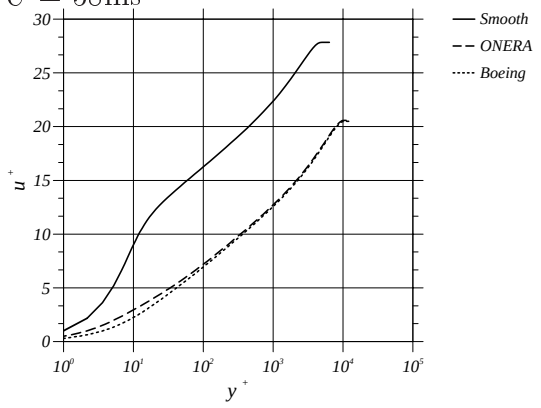

Figure 9: Semi-log plot of the velocity profiles predictions – MSU experiment – Hemispheres with spacing/height ratio of two – U = 58ms^{-1}

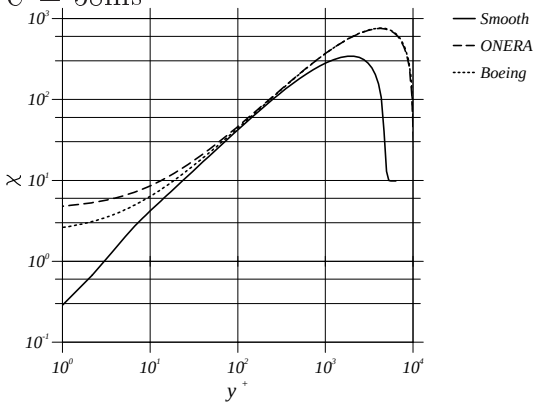

Figure 10: Logarithmic representation of $\chi = \frac{\tilde{\nu}}{\nu}$ predictions – MSU experiment – Hemispheres with spacing/height ratio of two – U = 58ms^{-1}

gradient flows. The equivalent sand grain height h_s is determined from Dirling's correlation.

The first surface is covered with hemispheres with a spacing of twice their height. For an external velocity of 12ms^{-1}, the reduced equivalent sand grain roughness height h_s^+ is about 45, i.e. a

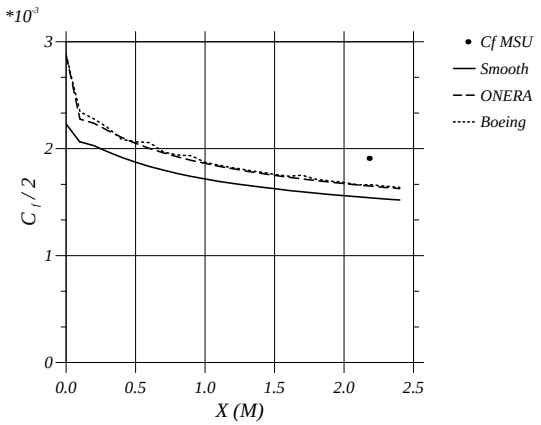

Figure 11: Skin friction predictions – MSU experiment – Hemispheres with spacing/height ratio of four – U = 12ms^{-1}

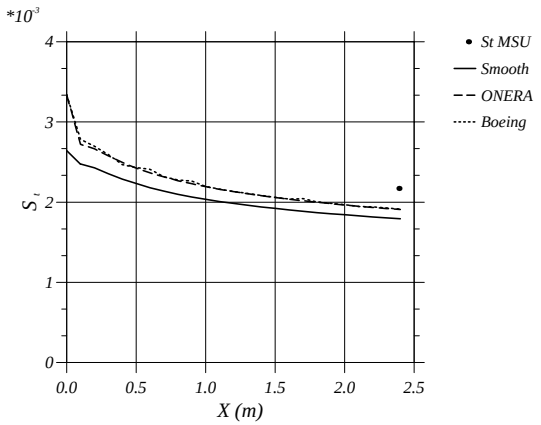

Figure 12: Stanton number predictions – MSU experiment – Hemispheres with spacing/height ratio of four – U = 12ms^{-1}

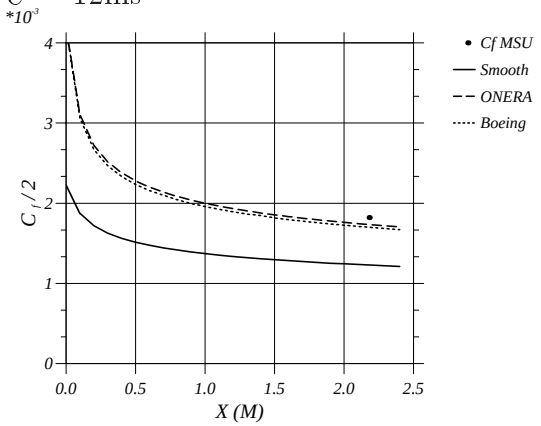

Figure 13: Skin friction predictions – MSU experiment – Hemispheres with spacing/height ratio of four – U = 58ms^{-1}

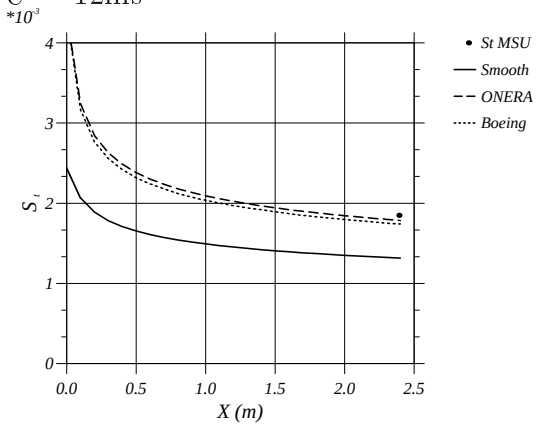

Figure 14: Stanton number predictions – MSU experiment – Hemispheres with spacing/height ratio of four – U = 58ms^{-1}

transitionally rough regime. Both extensions under-predict both the skin friction and the Stanton number, as shown in figures 5 and 6. Other roughness models yield similar predictions. Here again, ONERA's extension gives slightly higher and better levels than Boeing's. When the velocity is increased to 58ms^{-1}, the reduced equivalent sand grain roughness height h_s^+ is about 220, i.e. a fully rough regime. Then, the agreement between predictions and measurements is excellent, Boeing's predictions being slightly higher than ONERA's as shown in figures 7 and 8.

The velocity profiles in wall variables are plotted in figure 9. The shift Δu^+ of the logarithmic region and of the wake is about ten wall units. Both models give similar profiles, except very close to the wall where the notion of velocity profile makes little sense. Figure 10 evidences the increase of the quantity $\tilde{\nu}$ in the wall region. The two models take somewhat different values at the wall. In the logarithmic and wake region, they give similar eddy viscosity levels, reaching more than twice the level on a smooth surface (as a result of the increased boundary-layer thickness).

The second surface is covered with hemispheres with a spacing of four times their height. For an external velocity of 12ms^{-1}, the reduced equivalent sand grain roughness height h_s^+ is about 10, i.e. a transitionally rough regime. Both extensions give identical results but under-predict both the skin friction and the Stanton number, as shown in figures 11 and 12. Other roughness models

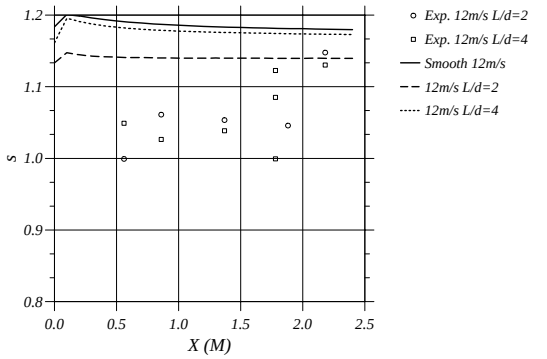

Figure 15: Analogy factor predictions – MSU experiment – U = 12ms^{-1}

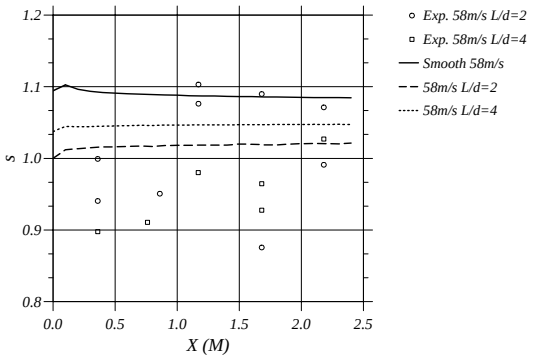

Figure 16: Analogy factor predictions – MSU experiment – U = 58ms^{-1}

yield similar predictions. When the external velocity is increased to 58ms^{-1}, the reduced equivalent sand grain roughness height h_s^+ is about 50, i.e. a transitionally rough regime similar to the first MSU case, but for a higher range of values of the Reynolds number R_θ based upon the boundary layer momentum thickness. As for the first MSU case, the skin friction is under-estimated while the Stanton number is fairly reproduced (figures 13 and 14).

Both extensions give similar predictions, whatever the roughness regime. Which extension gives a slightly higher skin friction depends upon the reduced equivalent sand grain roughness height h_s^+. The predictions are comparable to those of the best tested roughness models. As regards MSU experiments, for high values of h_s^+, predictions are in good agreement with experiments while roughness effects are under-estimated for the same surfaces in the transitionally rough regime. However, good predictions are achieved in the transitionally rough regime for Acharya et al. experiments. Either the relation $\Delta u^+(h_s^+)$ proposed by Nikuradse and which has been used to calibrate models is wrong and the good predictions in the transitionally rough regime are incidental, or a given roughness does not correspond always to the same equivalent sand grain roughness height, which means that the correlations are not accurate and complete enough.

A closer inspection of predictions reveals that the heat transfer increase due to roughnesses is overestimated compared to the skin friction increase. A striking example is the last test case for which the skin friction is under-estimated while the Stanton number is fairly predicted. This is a well-known drawback of the equivalent sand grain approach as the thermal and dynamical problems are solved similarly, the same increase being applied to the turbulent viscosity and conductivity. Assuming a linear relation between the velocity and total enthalpy profiles, the analogy factor s reads:

$$s = \frac{St}{C_f/2} \propto \frac{(\nu + \nu_t)\frac{\partial u}{\partial y}}{(\lambda + \lambda_t)\frac{\partial h_i}{\partial y}} \propto \frac{(\nu + \nu_t)}{(\lambda + \lambda_t)} \propto \frac{1}{P_m} \tag{17}$$

where P_m is a mixed Prandtl number which increases from the gas Prandtl number (0.72) for smooth surfaces to the turbulent Prandtl number (0.9) for fully rough surfaces. Figures 15 and 16 show that, although there is some scatter in the data, the decrease of the analogy factor is under-predicted by the models, compared with experiments, when the surface becomes rougher. This is consistent with Dipprey and Sabersky's results (1963) and the idea that the skin-friction increase is mainly due to pressure drag on the roughnesses while the heat-transfer increase is a viscous phenomenon and is more closely linked to the wetted surface increase. Therefore, the Reynolds analogy no longer holds for rough surfaces, while the modelling we implemented still uses it. Corrections based on functions of d/h_s may be devised in the future.

3 CONCLUSION

Two extensions of the Spalart–Allmaras turbulence model have been derived. Both assume a non zero-eddy viscosity at the wall and change the definition of the distance d, so that the model becomes non-local. Boeing's extension only uses the roughness height while ONERA's also refers to the friction velocity. The modifications are rather minor. The extensions can be used instead of the original S-A f_{t1} term to trip boundary layers; a rough band is placed along the transition line.

Tests on a variety of experiments show that these extensions give similar predictions, in fair agreement with other roughness models and, generally, with experiments. No test is available close enough to separation to differentiate the models for low skin friction levels. However, comparisons raise doubts about the universality of the equivalent sand grain which appears to depend upon the flow regime for a given surface. Moreover, the over-prediction of roughness effects on heat transfer compared with the effects on skin friction, using the equivalent sand grain approach and a uniform turbulent Prandtl number, is evidenced.

The first author wishes to acknowledge P. Baubias and G. Fontaine for their contributions.

REFERENCES

M. Acharya, J. Bornstein, and M.P. Escudier. (1986) Turbulent boundary layers on rough surfaces. *Experiments in Fluids*, 4(1):33–47.

B. Aupoix. (1994) Modelling of boundary layers over rough surfaces. In R. Benzi, editor, *Advances in Turbulence V*, pages 16–20, Sienna. Fifth European Turbulence Conference, Kluwer.

A. Blanchard. (1977) *Analyse Expérimentale et Théorique de la Structure de la Turbulence d'une Couche Limite sur Paroi Rugueuse*. PhD thesis, Université de Poitiers U.E.R.–E.N.S.M.A.

H.W. Coleman, B.K. Hodge, and R.P. Taylor. (1983) Generalized roughness effects on turbulent boundary layer heat transfer – A discrete element predictive approach for turbulent flow over rough surfaces. Air Force Armament Laboratory AFATL-TR-83-90, Mississippi State University.

D.F. Dipprey and R.H. Sabersky. (1963) Heat and momentum transfer in smooth and rough tubes at various Prandtl numbers. *International Journal of Heat and Mass Transfer*, 6:329–353.

R.B. Dirling, Jr. (1973) A method for computing rough wall heat transfer rates on reentry nosetips. AIAA Paper 73–763, AIAA 8^{th} Thermophysics Conference – Palm Springs, California.

R.M. Grabow and C.O. White.(1975) Surface roughness effects on nosetip ablation characteristics. *AIAA Journal*, 13(5):605–609.

M.H. Hosni, H.W. Coleman, J.W. Gardner, and R.P. Taylor. (1993) Roughness element shape effects on heat transfer and skin friction in rough-wall turbulent boundary layer. *International Journal of Heat and Mass Transfer*, 36(1):147–153.

M.H. Hosni, H.W. Coleman, and R.P. Taylor. (1991) Measurements and calculations of rough-wall heat transfer in the turbulent boundary layer. *International Journal of Heat and Mass Transfer*, 34(4/5):1067–1082.

J. Nikuradse. (1933) Strömungsgesetze in rauhen Rohren. Tech. Rept 361, VDI-Forschungsheft.

H. Schlichting. (1979) Boundary-layer theory. 7th Ed. McGraw-Hill, New York.

P. Spalart. (2000) Trends in turbulence treatments. AIAA Paper 2000-2306, Fluids 2000, Denver.

P.R. Spalart and S.R. Allmaras. (1994) A one-equation turbulence model for aerodynamic flows. *La Recherche Aérospatiale*, 1:5–21.

F.H.A. Tarada.(1987) *Heat Transfer to Rough Turbine Blading*. PhD thesis, University of Sussex.